Experiences with Hybrid Finite Elements in Geomechanics

Dieter Stolle & Peijun Guo
Civil Engineering – McMaster University, Hamilton, ON, Canada
Brandon Karchewski
Department of GeoScience – University of Calgary, Calgary, AB, Canada

GeoCalgary 2022 October 2-5 Reflection on Resources

ABSTRACT
Despite the belief in superior stress predictions by the hybrid finite element method during the early years, it did not become popular in geomechanics, likely because of limitations associated with nonlinear analysis and the additional computational steps that are required. Nevertheless, serviceability often controls the design of foundations. This implies that the conditions are far from the ultimate limit state and stress analysis based on small deformation elastic theory is most applicable. If there is an issue with an analysis it is the assumption of isotropy and not nonlinearity due to neglecting plastic strain hardening. An assumed stress hybrid framework is adopted in which all element stresses vary linearly, and pore pressures are constant. Performance comparisons are made with regular and hybrid formulations for a footing problem that examines the prediction of stresses due to a surface load and the gravity-driven creep of an ice slope that includes nonlinear flow. The object of this paper is to present a displacement-pressure (*u-p*) 4-node quadrilateral element that can handle the incompressibility of saturated soil and ice creep. This paper addresses how to handle body forces and nonlinearity.

RÉSUMÉ
Malgré la croyance en des prévisions de contraintes supérieures par la méthode des éléments finis hybrides au cours des premières années, elle n'est pas devenue populaire en géomécanique, probablement en raison des limitations associées à l'analyse non linéaire et des étapes de calcul supplémentaires nécessaires. Néanmoins, l'aptitude au service contrôle souvent la conception des fondations. Cela implique que les conditions sont loin de l'état limite ultime et que l'analyse des contraintes basée sur la théorie élastique des petites déformations est la plus applicable. S'il y a un problème avec une analyse, c'est l'hypothèse d'une isotropie et non d'une non-linéarité à cause de la négligence de l'écrouissage plastique. Un cadre hybride de contraintes supposées est adopté dans lequel toutes les contraintes des éléments varient linéairement et les pressions interstitielles sont constantes. Des comparaisons de performances sont faites avec des formulations régulières et hybrides pour un problème de semelle qui examine la prédiction des contraintes dues à une charge de surface et le fluage par gravité d'une pente de glace qui comprend un écoulement non linéaire. L'objet de cet article est de présenter une pression de déplacement (*u-p*) Élément quadrilatère à 4 nœuds qui peut gérer l'incompressibilité du sol saturé et le fluage de la glace. Cet article explique comment gérer les forces corporelles et la non-linéarité

1 INTRODUCTION

Engineers generally do not design for a structure to fail. Instead, they stay away from failure conditions as much as possible. An exception is perhaps slope stability. For the more usual situation, elastic solutions appear to be most suitable. If there is an issue, it is most likely the assumption of isotropy.

In the early years as hybrid formulations were introduced, there was a feeling that the corresponding finite elements would be superior relative to the displacement-based formulations given that local equilibrium is satisfied exactly. The acceptance of this approach never really did prevail given the challenges associated with handling nonlinear problems and body forces. It is also difficult to find literature that treats body forces. One exception is the contribution made by Karchewski et al. (2016).

The objectives of this paper are to address the matter of providing a further contribution dealing with body forces, demonstrate the treatment of a nonlinear constitutive law, and present a mixed displacement-pressure (*u-p*) analysis strategy that implements 4-node hybrid finite elements (MH-4) for problems in which full incompressibility is encountered. The theoretical background for hybrid elements is well established and may be found in Pian and Wu (2005) and the work of Bratianu (1980). Owing to the similarity of the field equations for the incompressible displacement formulation and those for creeping flow, the finite element formulation applies to both solid and creeping solid problems. Whereas displacement **u** and the shear modulus *G* characterize a solid's motion and material stiffness, respectively, the corresponding variables for fluids are velocity and viscosity η. Examples are presented dealing with an undrained short-term settlement under a footing and slope creep of ice.

1.1 Background

In geomechanics, large strain plastic deformations or creep strain rates are nearly or fully incompressible. During the early years of finite element development, there was a tendency to focus on the development of high-order

finite elements such as the 2-D 6- and 8-node isoparametric displacement elements. They performed better than the lower order ones that displayed volumetric locking and non-physical pressure variations for conditions approaching incompressibility. Chapter 4 of Hughes (2000) provides a nice overview of the causes of the pathological behaviors in low-order elements and of mitigation procedures.

The philosophy of favoring high-order elements has changed leading to the development of various volumetric strain and pressure enhancement techniques that mitigate the parasitic behavior of 4-node displacement elements; see, e.g., Detournay & Dzik (2006) and Bonet &Burton (1998). The preference for low-order elements lies largely in the greater flexibility to generate complex meshes and to incorporate adaptive finite element strategies.

A natural element for rectangular domains is the quadrilateral. Unfortunately, the conventional shape functions for the D-4 element are based on incomplete bilinear interpolation that leads to shear or volume locking; see Hughes (2000). Furthermore, non-physical pressure variations tend to accompany volumetric locking. These variations (checker-boarding) can be filtered via smoothening as shown by Sani et al, (1981). Nevertheless, smoothening hides the actual stress predictions that are tied to the displacement field including the non-physical pressures.

Mixed displacement-pressure (*u-p*) formulations show some success in dealing with incompressible boundary-valued problems. The 4-node quadrilateral with piecewise linear variations in displacement and constant pressure is the simplest element that can be implemented within the framework of mixed variational principles, cf. Hughes (2000). When a material is fully incompressible, this mixed element (M-4) satisfies the incompressibility constraint at the element level exactly in the average sense, although not locally. This element performs poorly for some problems, which necessitates smoothening techniques to recover the physical pressures.

According to Pian and Lee (1976), assumed stress hybrid elements are less susceptible to constraints on volume change. The strains are uncoupled from the displacement gradients thus mitigating the parasitic behavior. Thus, for an incompressible element, there is only one constraint that ensures that the volume of the element does not change, whereas, for the displacement formulation, the number of incompressibility constraints is the same as the number of integration points that are required for exact integration. It may also be argued that the stress field within a hybrid element is more realistic. Moreover, by selecting a complete polynomial approximation, the solution is invariant to the selection of the global coordinate system.

2 THEORETICAL PRELIMINARIES

2.1 Notation

To keep the exposition as simple as possible, we consider the deformation of an incompressible, 2-D isotropic, elastic solid that occupies an area A and unit thickness with boundary S on a single element. Using index notation, each point is represented by Cartesian location x_i with displacements u_i where $i \in [1, 2]$ or when using matrix notation by $\mathbf{x} = [x, y]^T$ with $\mathbf{u} = [u, v]^T$, cf. Malvern (1969) The comma operator is used to denote differentiation of a function f, i.e., $f_{,i} = \partial f / \partial x_i$.

Figure 1 shows a typical quadrilateral domain, where the origin of the local *x-y* system is placed at the geometric centroid. This selection has the attractive property that all first-order moments of an element domain vanish when constructing the volume integrals, *i.e.*, $\int x dA = \int y dA = 0$. Also included is the *s-t* natural coordinate system.

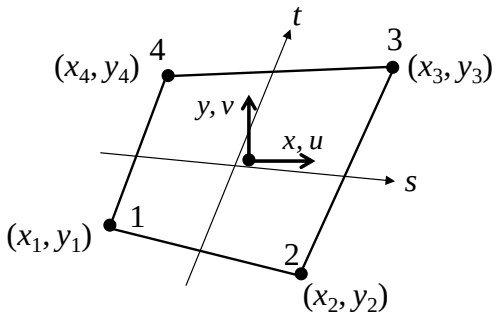

Figure 1: Quadrilateral element showing *x-y* and *s-t* coordinate systems.

2.2 Field Equations

We begin by considering a 2-D incompressible, plane-strain, saturated soil of unit thickness. Let us assume that the solid is in quasi-static equilibrium such that the total stress is given by $\sigma_{ij} = \sigma'_{ij} + p\delta_{ij}$, in which p is the pore pressure (mean normal stress) and σ'_{ij} represents the effective stress with δ_{ij} being the Kronecker delta. We may also write in Voigt/vector notation $\boldsymbol{\sigma} = \boldsymbol{\sigma}' + \mathbf{M}p$, with $\mathbf{M} = [1\ 1\ 0]^T$ representing the Kronecker delta. Given the body force ρg_i, the differential equation for equilibrium in the x_i direction is,

$$\sigma_{ij,j} + \rho g_i = 0 \rightarrow \mathbf{L}^T\boldsymbol{\sigma} + \rho\mathbf{g} = \mathbf{0} \qquad \text{in } A \qquad [1]$$

subject to stress and displacement boundary conditions

$$t_i = \sigma_{ij} n_j = \hat{t}_i \rightarrow \mathbf{t} = \mathbf{G}\boldsymbol{\sigma} = \hat{\mathbf{t}} \qquad \text{on } S_T \qquad [2]$$

$$u_i = \hat{u}_i \rightarrow \mathbf{u} = \hat{\mathbf{u}} \qquad \text{on } S_u \qquad [3]$$

with a caret implying prescribed tractions $\hat{t}_i$ on the surface S_T and displacements $\hat{u}_i$ on S_u. The matrix **L** is a linear differential operator operating on stress, which for two dimensions is $\boldsymbol{\sigma} = \left[\sigma_{xx}\ \sigma_{yy}\ \ \sigma_{xy}\right]^T$. The components of the unit normal to the surface are represented by n_j, which are contained in matrix **G**.

To the equilibrium equations, we add the relation between strain ε_{ij} and displacement u_i

$$\varepsilon_{ij} = \frac{1}{2}\left(u_{i,j} + u_{j,i}\right) \rightarrow \boldsymbol{\varepsilon} = \mathbf{L}\mathbf{u} \qquad [4]$$

as well as the that between effective stress and strain. For a saturated, incompressible elastic soil, we assume $\boldsymbol{\sigma}' = \mathbf{D}\boldsymbol{\varepsilon} \rightarrow \boldsymbol{\varepsilon} = \mathbf{D}^{-1}\boldsymbol{\sigma}'$ with $\boldsymbol{\sigma}'$ being the effective stress and $\mathbf{D}^{-1}$ the compliance matrix given by

$$\mathbf{D}^{-1} = \frac{1}{2G}\begin{bmatrix} 1-\nu & -\nu & 0 \\ -\nu & 1-\nu & 0 \\ 0 & 0 & 2 \end{bmatrix} \qquad [5]$$

in which G is the shear modulus and ν represents Poisson's ratio. When using engineering strain, $\boldsymbol{\varepsilon} = \left[\varepsilon_{xx}\ \varepsilon_{yy}\ \ \gamma_{xy}\right]^T$ with $\gamma_{xy} = 2\varepsilon_{xy}$ for 2-D.

2.3 Variations of Variables in Quadrilateral Element

The displacements and the strain field for the 4-node displacement element (D-4) are usually defined via $\mathbf{u} = \mathbf{N}\mathbf{a} \rightarrow \boldsymbol{\varepsilon} = \mathbf{B}\mathbf{a}$, in which **N** contains the bilinear interpolation functions for displacement that depends on natural coordinates (*s*-*t*) and **a** is a vector of nodal displacements with $\mathbf{B} = \mathbf{L}\mathbf{N}$ representing the strain-displacement matrix (Bathe 1996). Strictly speaking, displacement interpolation inside the domain of an element is not required for a hybrid formulation.

In what follows, the variation of the homogeneous solution for the effective stress within a hybrid element is approximated by using a complete linear polynomial for all stress components,

$$\boldsymbol{\sigma}' = \mathbf{P}\mathbf{b} \rightarrow \begin{bmatrix} \sigma_{xx} \\ \sigma_{yy} \\ \sigma_{xy} \end{bmatrix} = \begin{bmatrix} 1 & x & y & & & & \\ & & & 1 & x & y & \\ & -y & & & & -x & 1 \end{bmatrix} \begin{bmatrix} b_1 \\ \vdots \\ b_7 \end{bmatrix} \qquad [6]$$

with **b** containing the stress coefficients. When using complete polynomials, the predicated state of stress at a point is independent of a rotation of the frame of reference. It is important to emphasize that the approximation of $\boldsymbol{\sigma}'$ satisfies the homogeneous solution for the equilibrium equation exactly. The polynomial interpolation for mean normal stress (pore pressure) is constant.

2.4 Virtual versus Complementary Virtual Work

The virtual work for an incompressible saturated soil is given by

$$\int_A \delta\boldsymbol{\varepsilon}^T\left(\boldsymbol{\sigma}' + \mathbf{M}p\right)dA - \int_A \delta\mathbf{u}^T\rho\mathbf{g}dA - \int_{S_T}\delta\mathbf{u}^T\hat{\mathbf{t}}dS + \int_A \delta p\left(\mathbf{M}^T\boldsymbol{\varepsilon}\right)dA = 0 \qquad [7]$$

in which the strains are derived from the displacement gradients ($\boldsymbol{\varepsilon} = \mathbf{L}\mathbf{u}$) and the effective stresses are tied to strains ($\boldsymbol{\sigma}' = \mathbf{D}\boldsymbol{\varepsilon}$), with the strains tied to the displacement gradients. The surface tractions are not necessarily in equilibrium with the stresses and local equilibrium is not necessarily preserved.

On the other hand, the inherent assumptions for the modified complementary virtual work are that the stress field must satisfy local equilibrium (including body forces), the boundary tractions are in equilibrium with the stresses and the strains are directly related to the stresses and not to displacement gradients. A modified complementary potential energy (π_c) can be obtained from the total potential energy (π) via the relation,

$$\pi_c = \pi - \int_A \left(u_i\sigma_{ij}\right)_{,j}\,dA + \int_S u_i\sigma_{ij}n_j dS \qquad [8]$$

in which the two integrals correspond to 'integration-by-parts' and add up to zero. These integrals also prove to be useful for evaluating the surface integrals when dealing with triangular and quadrilateral elements as long as the approximating displacements satisfy the corresponding boundary variations.

The modified complementary virtual work for a saturated incompressible body is given by

$$-\int_V \delta\boldsymbol{\sigma}'^T\mathbf{D}^{-1}\boldsymbol{\sigma}'dV + \int_S \delta\boldsymbol{\sigma}'^T\mathbf{G}^T\mathbf{u}dS + \int_S \delta p\mathbf{M}^T\mathbf{G}^T\mathbf{u}dS - \int_S \delta\mathbf{u}^T\mathbf{G}\boldsymbol{\sigma}'dS - \int_S \delta\mathbf{u}^T\mathbf{G}\mathbf{M}pdS - \int_S \delta\mathbf{u}^T\mathbf{G}\boldsymbol{\sigma}_p dS - \int_{S_T}\delta\mathbf{u}^T\hat{\mathbf{t}}dS = 0 \qquad [9]$$

with $\boldsymbol{\sigma}_p = \left[0\ \ -\rho g y\ \ 0\right]^T$ being the particular solution of the equilibrium equation of the body force term. The body force and pressure terms enter Eq. (9) by recognizing that the

total stress along the boundary S of an element is $\boldsymbol{\sigma} = \boldsymbol{\sigma}' + \mathbf{M}\,p + \boldsymbol{\sigma}_p$. An examination of this equation reveals that displacement variations are only required along the boundary and that the equilibrating distributions of stress and pressure are required only within each element. This does not imply that stresses are continuous between elements. By applying integration by parts, it is possible to show that the body force terms of Eqs. (9) and (10) are the same, although in one case we have an area integral and in the other a contour integral.

2.5 Mixed Hybrid Formulation

Given that mixed formulations based on Eq. (7) are well established, we summarize only the mixed formulation based on Eq. (9). It is assumed that the effective stress varies linearly $\boldsymbol{\sigma}' = \mathbf{P}\mathbf{b}$ and p is constant within A, and $\mathbf{u} = \mathbf{N}\mathbf{a}$ along the boundary S. We convert Eq. (9) to

$$\begin{bmatrix} \mathbf{L}_u^T\mathbf{H}\mathbf{L}_u & \mathbf{L}_p^T \\ \mathbf{L}_p & 0 \end{bmatrix} \begin{bmatrix} \mathbf{a} \\ p \end{bmatrix} = \begin{bmatrix} \mathbf{f}_g + \mathbf{f}_t \\ 0 \end{bmatrix} \qquad [10]$$

in which $\mathbf{H} = \int_V \mathbf{P}^T\mathbf{D}^{-1}\mathbf{P}dV$, $\mathbf{L}_u = \int_S \mathbf{P}^T\mathbf{G}^T\mathbf{N}dS$, $\mathbf{L}_p = \int_S \mathbf{M}^T\mathbf{G}^T\mathbf{N}dS$, $\mathbf{f}_g = \int_S \mathbf{N}^T\mathbf{G}\boldsymbol{\sigma}_p dS$ and $\mathbf{f}_t = \int_{S_T} \mathbf{N}^T\hat{\mathbf{t}}dS$.

The global matrix equivalent of Eq. (10) is formed by taking into account inter-element compatibility and equilibrium, or by invoking the extensive thermodynamic property of energy.

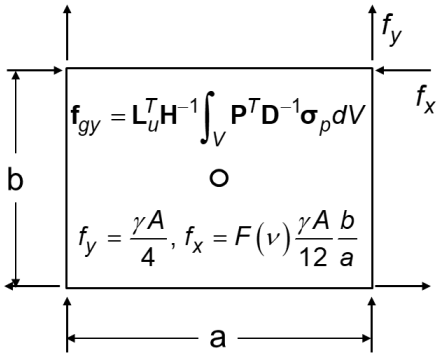

Figure 2: Gravity loading for rectangular element.

It should be noted that Karchewski (2015) and Karchewski et al. (2016) include an additional gravity loading term that is associated with the area integral, shown in Figure 2. Referring to this figure, we observe for a simple rectangular element that gravity loading in the y-direction results in forces in the x-direction, as well as couples that cancel. The corresponding horizontal forces are a function of Poisson's ratio and the aspect ratio of the element. For a uniform mesh such as used for Example 1, this term would not contribute to the global load vector, if gravity were to be included.

For an incompressible solid, $\boldsymbol{\sigma}'$ is replaced by the deviatoric stress **S,** and the constitutive law is simplified to $\mathbf{S} = 2G\boldsymbol{\varepsilon}$; see, e.g., Malvern (1969). We may also write $\mathbf{S} = \mathbf{D}\boldsymbol{\varepsilon}$ and use engineering strain. The same approximations are adopted as for the saturated, incompressible soil.

The difference between the exposition just presented for undrained soil response and that for an incompressible solid, lies mainly in the formation of the **D**-matrix which allows for a compressible elastic soil skeleton subject to an incompressibility constraint, and the interpretation of p. The pore pressure p now takes on the role of mean normal stress. An important reason for considering the virtual work expressions is that they apply to nonlinear problems. There are various possibilities for taking into account the nonlinearities when updating the stress or strain-dependent properties. The one proposed here is to assume the nonlinear constitutive law for an element is determined by the stress/strain conditions at the geometric centroid, which represents an "average". For strain dependence of the constitutive law, we can also obtain average strains $\bar{\boldsymbol{\varepsilon}}$ by performing contour integrals around an element, i.e.,

$$\bar{\boldsymbol{\varepsilon}} = \frac{1}{A}\oint \mathbf{G}^T\mathbf{N}dS\,\mathbf{a} \qquad [11]$$

that allows us to estimate average properties.

3 NUMERICAL EXAMPLES

Modern day finite element modeling generally involves relatively fine meshes when compared with those used in the early years. The non-physical pressure distributions are however much more apparent with solutions based on coarse grids than are those obtained using finer discetization. Data processing techniques that have found their way into the commercial software tend to often hide any parasitic behaviour that may be present.

Two plane strain examples are considered: a footing problem that demonstrates the prediction of mean normal stress (pore pressure) and shear stress under the footing; and the flow of the northeast slope of the Barnes Ice Cap (BIC) (Hooke et al. 1979). Given the plane strain assumption, the mean effective and shear stresses correspond to the center and radius of Mohr's circle, respectively. These represent stress invariants for plane strain problems. The sign convention for pressure is tension positive. Stresses are calculated at the geometric centroid of the hybrid element (MH-4), where the true average values are obtained. For the assumed displacement elements, they are determined at the origin of the natural coordinate system. This location provides the most reasonable stresses for the D-4 element. The letters M, D and H denote mixed, displacement and hybrid

formulations with the number representing the number of nodes

3.1 Frictionless Footing Subjected to Vertical Pressure

We have an example of a 5 m wide footing that uniformly loads the top of a 5 m thick by 20 m wide soil deposit with a -8000 kPa pressure. Owing to symmetry only half the problem is analyzed with a 20 ×20 mesh. There is full fixity along the bottom and along the RHS vertical boundary, with rollers along the LHS boundary to accommodate the symmetry. The full fixity along the outside boundaries represents an extreme condition when a material response is incompressible. As indicated, pore pressures are constant in the HM elements, with piecewise linear interpolation of displacements along the boundary. The elastic modulus and Poisson's ratio are 100,000 kPa and 0.3, respectively.

Figure 3 shows the 'smoothened' excess pore pressure distribution, as well as the 'magnified' deformed mesh. The scale is provided in the figure caption. For this example, it turns out that the least-squares smoothened pressure predictions by the HM-4 and DM-4 formulations were found to be very similar. The mean effective stress increases were close to zero. It must be understood that no increase in the mean effective stress developed due to the fluid being completely incompressible. This may be proven for an isotropic soil at the constitutive level. On the other hand, when considering the pore pressure changes that are predicted when using stress-path-dependent 'pore pressure' parameters to account for 2 or 3-D stress variations this may be unexpected. We also observe that under the load, the soil surface moves vertically down with it rising along the free surface, which is what one should expect for an incompressible medium. The deformations are shear dominated.

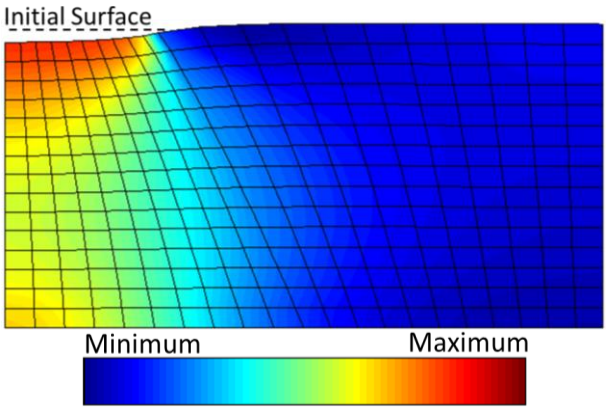

Figure 3: Excess pore pressure distribution due to surface loading. (Minimum = 0 kPa, Maximum = 150 kPa)

Although not shown, there are some numerical issues that should be mentioned. The mixed formulations did exhibit checkerboarding of predicted pressures. There were two main observations: as the number of elements increased, the errors became smaller; and selective integration appeared to mitigate the non-physical pressure modes but does not eliminate them entirely. This observation is consistent with the trend described by Bathe (1996), who provides a detailed discussion on spurious pressure modes in Chapter 4 of his textbook.

Smoothening was found to be effective in recovering the physical pressure field. It should be noted that the 8-node isoparametric quadrilateral element with reduced integration, which is popular in geomechanics, was found to also have issues with non-physical pressure variations.

Figure 4 illustrates the increase in shear as represented by the radius (t) of Mohr's circle. The colour coding is the same as that shown in Figure 3, with the respective minimum and maximum limits being presented in the figure caption. Once again, the smoothened HM-4 and DM-4 predictions were found to be very close. As one might expect, the maximum shear which is responsible for the instantaneous 2-D surface settlements was maximum under the footing, but not immediately along the soil-footing interface. The upward movement of the surface is attributed to the incompressibility constraint condition, not the changes in stress.

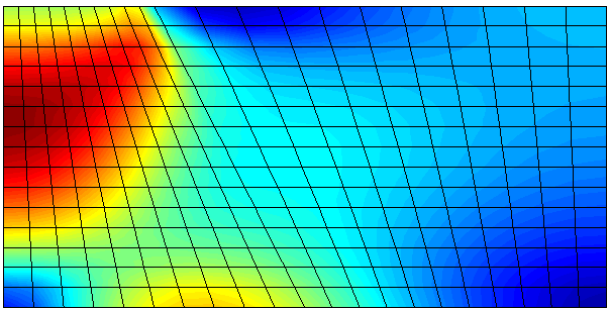

Figure 4: Equivalent shear stress increase due to surface loading. (Minimum = 0 kPa, Maximum = 50 kPa)

This example demonstrates that the two mixed formulations (HM-4 and DM-4) provided similar predictions. These elements were found to be less susceptible to locking when compared to predictions by regular displacement elements with Poisson's ratio approaching half. Nevertheless, the mixed elements are not immune to spurious pressure variations. In the example that follows, the emphasis is on the performance of the hybrid mixed formulation for the case of gravity-driven flow. We also address the solution of stress/strain-rate dependent flow.

3.2 Gravity Driven Flow

3.2.1 Constitutive Description

Restricting ourselves to incompressible, two-dimensional flow with pressure insensitive, isotropic material behaviour, the relation between deviatoric stress and strain rate takes the form $\mathbf{S} = 2\eta\dot{\boldsymbol{\varepsilon}}$ with η being the viscosity and the dot above a symbol implying a time derivative. Although engineering strain rate is adopted in this paper, it should be noted that this form of constitutive law implies that

$\dot{\varepsilon}_{xy} = \dot{\gamma}_{xy}/2$. For incompressible problems the volumetric strain rate $\mathbf{M}^T\dot{\boldsymbol{\varepsilon}}$ vanishes; thus, the deviatoric strain rate is the same as the total strain rate.

For creep flow, Glen's (1955) power law is most often adopted. It is convenient to write it as $\dot{\varepsilon}_e = A(\sigma_e/p_a)^r$, which leads to the following relation for viscosity

$$\eta = \frac{1}{3}\frac{\sigma_e}{\dot{\varepsilon}_e} \qquad [12]$$

where $\sigma_e = \sqrt{\frac{3}{2}\mathbf{S}^T\mathbf{S}}$ and $\dot{\varepsilon}_e = \sqrt{\frac{3}{2}\dot{\boldsymbol{\varepsilon}}^T\dot{\boldsymbol{\varepsilon}}}$ are Dorn's definitions for the equivalent stress and equivalent strain rate, respectively, and p_a is a reference pressure assumed to be 100 kPa, with r and A being material properties that depend on temperature. For visco-plasticity Zienkiewicz and Godbole (1974) recommend the relation

$$\eta = \bar{\eta} + \frac{2c}{\dot{\varepsilon}_e} \qquad [13]$$

in which $\bar{\eta}$ is a reference viscosity and c represents the shear strength of the material. A limit must be placed on the viscosity since $\eta \to \infty$ as $\dot{\varepsilon}_e \to 0$. A reasonable limit is $\eta \le 2000\bar{\eta}$.

The standard material properties adopted in this paper for the simulations of ice creep are unit weight γ = 8.952 kN/m^3, Poisson's ratio v = 0.5 and the creep law exponent r = 3. The solution procedure takes into account that the nonlinear creep law is based on the direct iteration method involving the general algorithm $\mathbf{K}(\dot{\boldsymbol{\varepsilon}}_{en})\mathbf{a}_{n+1} = \mathbf{F}$, in which **K** is the "stiffness" matrix, **a** contains the unknown velocities and pressures and n is an iteration counter. When carrying out the analyses, convergence was based on the root mean square error of the velocities being less than 0.0001. To ensure convergence the viscosity, assumed constant for an element, was expressed in terms of strain rate, not stress.

3.2.2 Barnes Ice Cap, Baffin Island

The Barnes Ice Cap (BIC) has been of interest to glaciologists for many years because parts of the ice mass have a history of becoming unstable, a phenomenon referred to as surging. Finite element simulations have been performed for this structure in the past; see, e.g., Hooke et al. (1978) and Stolle (1988). The purpose of the following simulations was to test the formulations on a problem that is of a considerably different scale than is usually encountered in engineering. It takes into account a nonlinear creep law with a varying creep coefficient A. The geometry, boundary conditions, and structure of the FEM mesh of the northeast slope are shown in Figure 5, along with the measured horizontal surface velocities. The mesh that was used to generate the results shown herein was for a finer mesh (118 × 8). It should be noted that simulations were also performed with a 6-node velocity-pressure triangular element (DM-6), in which pressure was continuous between elements.

Figure 6 provides the distribution of the A-parameter in the creep law as a function of the horizontal distance along the ice cap. The distribution was obtained via calibration with the measured horizontal surface velocities. Although no attempt was made to optimize the parameters, which depend on temperature, the calculated surface velocities are shown to provide the correct trend (see the top left side of Figure 5). Preliminary analysis revealed that the average relative difference in the prediction of shear stress between HM-4 and DM-4 was 7 percent when comparing values element by element, with the corresponding difference for pressure being 1 percent. As a result, the smoothened stress predictions were found to be very good.

A series of simulations were also performed assuming power-law creep with constant coefficients. The predicted variations in pressure and maximum shear stress reflected by the contour plots tended to vary smoothly. Figure 7 shows the smoothened pressure and shear stress distributions for the case where the coefficient varied with the distance along the glacier. As might be expected, the pressure variation is fairly smooth. On the other hand, the spatial distribution of shear does not appear to be as regular, being more sensitive to the flow law. The reader should however keep in mind that the scales for the horizontal and vertical axes are different as shown in Figure 5. More important for the present discussion is that the contours from the three formulations are virtually identical, particularly for the predictions stemming from the DM-4 and HM-4 elements. An observation of significance is that the σ_{xy} shear contour of 40 kPa intersects the divide. This is not possible due to the boundary condition but is the result of the contour plotting algorithm. Nevertheless, all three formulations are shown to predict the same stress variations after smoothening.

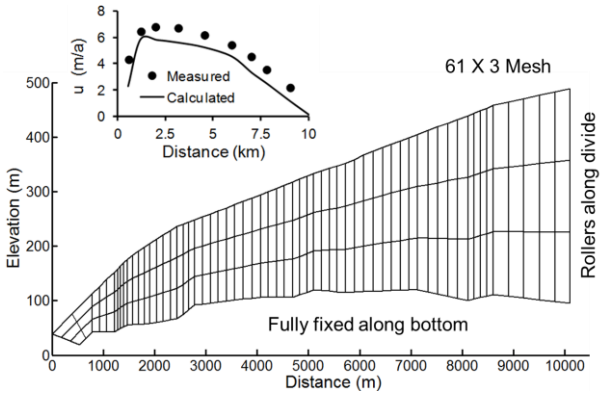

Figure 5: BIC example – (top) measured and predicted surface velocities (meters per annum), and (bottom) geometry of ice mass and representative mesh for quadrilateral elements.

Our final comparison for this example deals with the magnitude of the total velocity for the three formulations. The contours for the three are shown in Figure 8. Once again, the overlap of the three sets is excellent. It should be noted that, had the creep law been uniform (implying a constant *A*-parameter), then the maximum would have occurred closer to the divide, i.e., in the vicinity of the 8 km location.

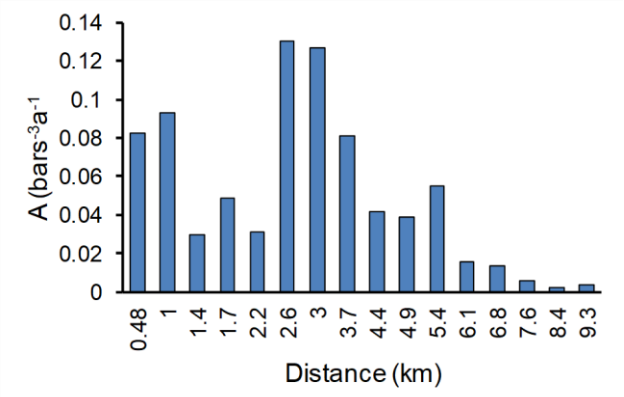

Figure 6: Variation of A-parameter with respect to distance along the ice cap.

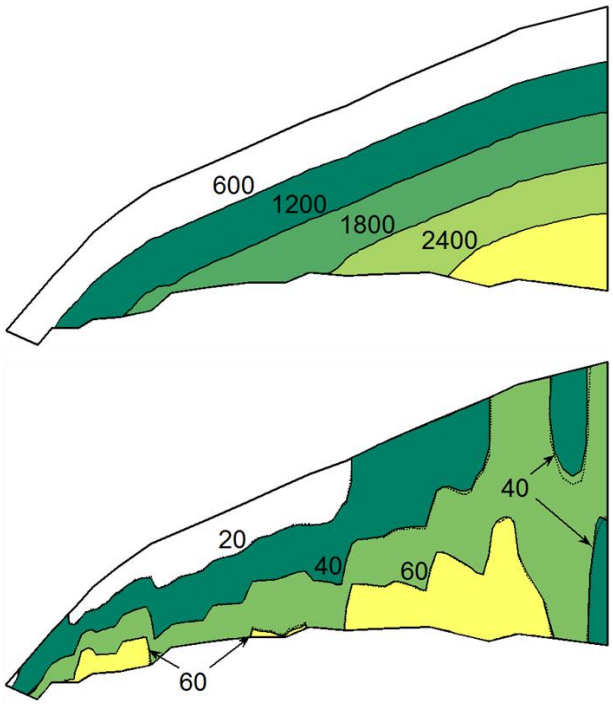

Figure 7: Comparison of creep predictions by HM-4, DM-4 and DM-6 models for (top) mean normal stress in kPa, (bottom) shear in kPa. The DM-6 prediction is denoted by dotted lines, and HM-4 and DM-4 by solid lines.

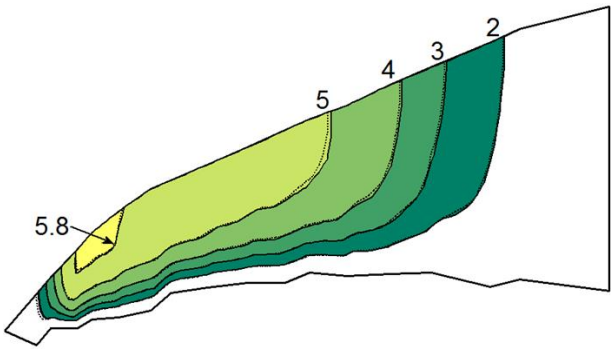

Figure 8: Total velocity contours by HM-4, DM-4 and DM-6 models.

4 CONCLUDING REMARKS

The authors have been involved in research dealing with the implementation of assumed stress polygonal elements, an attractive feature of these elements being that equilibrium is satisfied within each element. A scouting expedition was carried out for this paper to investigate the performance of the 4-node mixed hybrid element for situations in which the deformations are incompressible, as well as for predictions involving nonlinear constitutive behaviour and gravity driven flow. While nonlinear FEM is well established for regular displacement formulations, the literature regarding nonlinear analysis with assumed stress elements is relatively scarce. It had originally been assumed that the hybrid element (HM-4) would perform better than the corresponding displacement element (DM-4).

An important finding is that the predictions from both 4-node elements were almost identical, particularly after smoothening the stresses. The implementation of the hybrid element, where all stress components varied linearly, however, has the advantage of being able to better capture variations in shear stress σ_{xy} when compared to the bilinear displacement element, although the differences are often small when making comparisons of the average stresses in an element. The 4-node, mixed assumed stress formulation is not capable of avoiding the 'checkerboard syndrome', at least for the implementation that was investigated. This was not surprising given the origin of the “syndrome’. Nevertheless, the checker-boarding was not a problem for the gravity-driven deformation phenomenon that was considered in this paper. With regard to gravity loading, although the integral equations to obtain the load vector are different, it can be shown that they provided the same load vector, at least for the low-order elements.

Although the stress predictions are better when using the mixed hybrid (HM-4) element, the D-4 element with selective integration for the volumetric stiffness and DM-4 mixed element were found to be easier to implement. Given the trend to adopt low order elements with fine discretization, the gains in improved stress prediction that have been reported for the hybrid elements when using coarser meshes are not realized after smoothening the

predictions for plotting purposes. This observation does not necessarily apply for analyzes based on unstructured meshes consisting of polygonal elements with an arbitrary number of nodes.

5 ACKNOWLEDGEMENTS

The authors would like to thank Natural Sciences and Engineering Research Council of Canada for their funding contribution to this project.

6 REFERENCES

Bathe, K.J. 1996. *Finite Element Procedures*, Prentice-Hall Englewood Cliffs, NJ,

Bonet, J. and Burton, A.J. 1998. A simple average nodal pressure tetrahedral element for incompressible and nearly incompressible dynamic explicit applications, *Communications in Numerical Methods in Engineering*, 14:437–449.

Bratianu, C. 1980. *Hybrid and Mixed Finite Element Models for Viscous, Incompressible Flows*, Doctoral Dissertation, School of Nuclear Engineering, Georgia Institute of Technology, 145 pages.

Detournay, C. and Dzik, E. 2006. Nodal Mixed Discretization for Tetrahedral Elements, *4th International FLAC Symposium on Numerical Modeling in Geomechanics*.

Glen, J.W. 1955. The Creep of Polycrystalline Ice, *Proceedings of the Royal Society, Series A*, 228:519–538.

Hooke, R.L., Raymond, C.F., Hotchkiss, R.L. and Gustafson, R.J. 1979. Calculations of velocity and temperature in a polar glacier using the finite element method, *Journal of Glaciology*, 24:131–146.

Hughes, T.J.R. 2000. *The Finite Element Method: Linear Static and Dynamic Finite Element Analysis*. Dover Publications Inc.

Karchewski, B. 2015. *Multi-scale Modelling of Geomechanical Behaviour Using the Voronoi Cell Finite Element Method (VCFEM) and Finite-Discrete Element Method (VCFEM-DEM)*, Ph.D. Thesis, Department of Civil Engineering, McMaster University, 222 pages.

Karchewski, B., Pekinasova, A., Stolle, D., and Guo, P. 2016. Investigation of a Hybrid Polygonal Finite Element Formulation for Confined and Unconfined Seepage, *International Journal for Numerical and Analytical Methods in Geomechanics*, 40: 1643– 1661.

Malvern, L.E. 1969. *Introduction to the Mechanics of a Continuous Medium*. Prentice-Hall, Englewood Cliffs, NJ.

Pian, T.H.H. and Lee, S.W. 1976. Notes on Finite Elements for Nearly Incompressible Materials*, AIAA Journal*, 16(6): 824-826.

Pian, T.H.H. and Wu, C.C. 2005*. Hybrid and Incompatible Finite Element* Methods, Chapman & Hall/CRC, New York.

Sani, R.L., Gresho, P. M., Lee, R.L. and Griffiths, D.F. 1981. The Cause and Cure of the Spurious Pressures Generated by Certain FEM Solutions of the Incompressible Navier-Stokes Equations: Part 1, *International Journal for Numerical Methods in Fluids*, 1:17–43.

Stolle, D.F.E. 1988. A One-Dimensional Finite Element Model for Two-Dimensional Glacier Flow. *Journal of Glaciology*, 34:1–6.

Zienkiewicz, O. C. and Godbole, P. N. 1974. Flow of Plastic and Visco-plastic Solids with Special Reference to Extrusion and Forming Processes, *International Journal for Numerical Methods in Engineering* 8 (1): 1–16

Zienkiewicz, O.C. and Taylor, R.L.1989. *The Finite Element Method,* 4th ed., Vol. 1, McGraw-Hill, U.K.